Variational Transition State Calculations of the CH_2F_2 + OH Hydrogen Abstraction Reaction

Angels González-Lafont,*,† José M. Lluch,† and Joaquín Espinosa-García‡

Departament de Química, Universitat Autònoma de Barcelona, 08193 Bellaterra, Barcelona, Spain, and Departamento de Química Física, Universidad de Extremadura, 06071 Badajoz, Spain

Received: July 11, 2001; In Final Form: September 21, 2001

We present variational transition state calculations of the rate constants for the CH_2F_2 + OH hydrogen abstraction reaction in the temperature range from 200 to 500 K. We have employed a dual-level approach to direct dynamics using the interpolated optimized corrections methodology. In the variational transition state calculations, tunneling has been included within the microcanonical optimized multidimensional scheme employing the recently developed LCG4 (large-curvature ground-state, version 4) approximation to evaluate the large curvature tunneling effects. At the QCISD(T)/6-311++G(2df,p)//QCISD/6-311G(d,p)[QCISD/6-31G(d)]///PM3 and the CCSD(T)//MP2/cc-pVTZ///PM3 levels, the classical energy barriers turn out to be, respectively, 5.8 and 5.1 kcal/mol. These calculations show significant variational effects at all temperatures. These direct dynamics approaches reproduce quite well the experimental rate constants from 500 to 250 K, and slightly overestimate them from 250 to 210 K. The disagreement at the low-temperature range needs of further analysis.

Introduction

Chlorofluorocarbons (CFCs) have been widely used as aerosol spray propellants, refrigerants, or in foam blowing applications. However, it is now well known that CFCs have long tropospheric lifetimes and can be transported to the stratosphere where they are involved in the depletion of the ozone layer. Because they are inert, these compounds also accumulate in the atmosphere with the potential implication for global warming. Thus, a very important international effort has been undertaken to find environmentally acceptable alternatives to CFCs, especially since the production of CFCs was restricted under the Montreal protocol[1] on substances that destroy stratospheric ozone. In contrast to CFCs, the presence of hydrogen atoms in hydrofluorocarbons (HFCs) makes them reactive toward hydroxyl (OH) radicals in the troposphere, minimizing or avoiding their transport to the stratosphere.[2] Consequently, most of these compounds present considerably shorter tropospheric lifetimes than CFCs, although HFCs may be potent greenhouse gases due to the strong IR activity of the C−F bonds and, therefore, it is important to have good estimates of their atmospheric lifetimes to really assess their environmental impact. On the other hand, HFCs contain neither chlorine nor bromine and so have no ozone depletion potential associated with the established chlorine- and bromine-based catalytic ozone destruction cycles. For these two environmental advantages over CFCs, HFCs are currently being used as substitutes for CFCs in many industrial applications.

Chlorofluorobromocarbons (or halons) are the major fire suppression agents for use in confined spaces or to protect electronics. However, in due time, it was recognized that the bromine-containing halons were also destructive to the stratospheric ozone layer, even more so than CFCs on a molecule-to-molecule comparison basis. In fact, halons as a class became the first group of compounds whose production has already been halted. Among the compounds proposed as suitable replacements for halons are HFCs, since they do not contribute to ozone depletion or significantly to global warming, as stated in the previous paragraph, and are also known to have some fire suppression ability. In particular, among the hydrocarbons, fluorinated methanes are considered to be safe alternative potential candidates as flame suppressants.[3]

The key removal process for HFCs in the troposphere is the abstraction reaction of hydrogen atom by hydroxyl (OH) radical, and this process is also one of the major destruction pathways of the combustion reactions that take place in a flame. For these reasons, in the past decade, that abstraction reaction has attracted considerable attention from both experimentalists and theoreticians. Since the values of the atmospheric lifetimes for HFCs, needed to infer if the partially fluorinated hydrocarbons are really environmentally safe replacements of CFCs and halons, rely on the accuracy of the experimental and calculated rate constants for the abstraction reaction by OH, continuous search is underway trying to improve the experimental techniques and the theoretical methodologies that deal with the kinetics of those reactions. To this aim, the hydrogen abstraction reactions by OH from fluoromethanes (CH_3F, CH_2F_2,CHF_3), which are the smallest compounds among HFCs, are the most suitable processes for modeling and testing methodologies that could be applied to larger molecules or to the complete reaction kinetic schemes for the degradation of HFCs.

In a previous work,[4] we performed dynamics calculations for the CH_3F + OH reaction using variational transition state theory (VTST) with the inclusion of multidimensional tunneling (MT) effects. The conclusions of that paper indicated the following. (1) The enthalpy of reaction and the barrier height strongly depend on the level of electronic calculation and, particularly, of the basis set. (2) Variational effects are significant due to

* Corresponding author. Phone 34-935811672; Fax 34−935812920; E-mail: angels@klingon.uab.es.
† Universitat Autònoma de Barcelona.
‡ Universidad de Extremadura.

10.1021/jp012648j CCC: $20.00
Published on Web 10/26/2001

the flat potential energy surface (PES) of this process. So, differences between conventional transition state rate constants and variational transition state rate constants have been obtained. (3) Tunneling plays an important role in this reaction, although this effect was overestimated in our calculations, especially at low temperatures. In any case, the curvature observed experimentally in the Arrhenius plot is still an open question because the temperature dependence has not been sufficiently studied. (4) Dual-level dynamics based on semiempirical molecular orbital calculations seem to be, because of their economy and the quality of their results, a very promising tool for computing dynamical properties in reactions with halocarbons.

Concurrent to our work, Schwartz et al.[5] published a computational study of the kinetics of hydrogen abstraction by the hydroxyl radical from methane and its fluoroderivatives. In that investigation, the authors use conventional transition state theory (TST) to calculate the reaction rate constants, and tunneling is evaluated using a monodimensional Eckart potential energy function. Schwartz et al.[5] show that Eckart tunneling effects calculated using the HF/6-31G(d) imaginary frequency at the saddle point give an excess of curvature in the Arrhenius plot while the tunneling efficiency is drastically reduced when the imaginary frequency used is obtained from an Eckart fit to G2 energies along the MEP. The fitted imaginary frequencies ($1165i - 1382i\ cm^{-1}$) are much lower (approximately a factor of 2.5) than the HF frequencies ($2900i\ cm^{-1}$) and more than 60% when compared to the QCISD/6-311G frequencies ($\sim 1885i\ cm^{-1}$), reflecting a broader MEP at the G2 level. Then, the tunneling factors were recalculated by the authors on an Eckart adiabatic profile constructed by adding the zero point energies (ZPEs) for reactants, products, and the transition state to the classical energy and by readjusting slightly the imaginary frequency of the Eckart function. The calculated TST rate constants are systematically lower than the experimental results for all of the reactions, except for $CH_4 + OH$ at elevated temperatures. Finally, the classical barrier heights were adjusted for the four reactions to require that $k_{TST} = k_{exp}$ at 298 K and the adjusted rate constants show in general a very good agreement with experimental results at all temperatures for which measured rates are available. The authors conclude that fitting the high level PES is the only currently feasible procedure for calculating accurate tunneling factors because incorrect values of the reaction path imaginary frequency constitute the greatest source of error in the calculation of the tunneling factors for hydrogen atom abstraction reactions.

More recently, Korchowiec et al.[6] have published another study on the hydrogen abstraction reaction from methane and hydrofluoromethanes by the OH radical. The main aim of that work is also to find a general methodology that correctly describes the kinetics and thermodynamics of those hydrogen abstraction reactions. The rate constants are calculated according to conventional transition state theory, and tunneling is neglected or included with the Wigner correction formula, assuming no significant curvature on the Arrhenius plots for the four reactions. The reaction enthalpies and the activation energies are calculated using several G2 type schemes. The authors conclude that the G2M scheme (where the geometries and ZPEs are calculated at B3LYP/6-311G(d,p) level) gives accurate reaction enthalpies. The influence of fluorine substitution is also correctly, at least qualitatively, described. For the activation energies, the values calculated with the G2M barrier heights and using the Wigner tunneling correction, with an average deviation of 0.95 kcal/mol, show the best agreement with the experimental activation energies among the different methods used by the authors. The influence of fluorine substitution on the activation energies is also qualitatively reproduced. However, Korchowiec et al.[6] do not give in their paper any direct comparison between experimental and theoretical rate constants.

Using the same methodology, TST plus Wigner's tunneling correction, Louis et al.[7] have recently carried out rate constant calculations over the temperature range 250−400 K for the H-abstraction reactions from a series of 12 halogenated methanes by the hydroxyl radical. Their results suggest that the PMP4-(SDTQ)/6-311G(3df,2p)//MP2/6-311G(2d,2p) level of electronic structure calculation is a good compromise between accuracy and computational expense for the theoretical treatment of hydrogen abstraction reactions between OH radicals and halomethanes. However, large deviations from the experimental values observed in one case make the authors suggest that VTST and more sophisticated models for tunneling corrections may be the methodologies of choice.

In view of those last results with TST/Wigner methodology for the rate constant calculation of hydrogen abstraction reactions from halomethanes, the aim of this work is to show how reliable VTST/MT can be when trying to reproduce experimental rate constant values of H-atom abstraction reactions from halomethanes without any previous fitting to experimental results. We have taken, as a second example, the $OH + CH_2F_2$ reaction in order to confirm if our previous conclusions on these hydrogen-atom abstraction reactions are still valid.

Method of Calculation

The rate constants calculated in this work have been obtained using a dual-level approach to direct dynamics. In this methodology, low level electronic structure calculations are carried out at a large number of geometries to generate a wide representation of the PES. Then, at some selected points of the PES, higher level electronic structure calculations are used to correct the low level information on the PES. We will present first in this section the electronic structure calculations and, second, the details of the dynamics calculations.

Electronic Structure Calculations. The low level PES was obtained using the semiempirical PM3-NDDO Hamiltonian.[8] On the PM3 PES, the geometries of the stationary points for the $OH + CH_2F_2$ reaction were located and characterized using first and second derivatives. In addition, the stationary points were also found and characterized using the AM1 semiempirical method.[9] The PM3 minimum energy path (MEP) was calculated using the Page−McIver algorithm[10] with a gradient step-size $\delta s = 0.005$ au (where s denotes the distance along the MEP in an isoinertial mass-scaled coordinate system with a scaling mass equal to 1 amu). The force constant matrices were computed in steps of 0.01 au along the MEP. The numerical second derivatives in this work were evaluated using the adaptive step size scheme included in MOPAC 5.09mn subroutines.[11] The normal-mode analysis was performed in redundant curvilinear coordinates (six stretches, eight angles, and four dihedrals).[12] The advantage of curvilinear coordinates over the rectilinear ones is that in some cases the lowest bending frequencies had unphysical imaginary values over a wide range of the reaction coordinate due to the rectilinear coordinates. All vibrations have been treated within the harmonic approximation except for the internal rotation motion corresponding to the lowest mode at the saddle point and along the MEP. For this mode we have used the hindered rotor approximation of Truhlar and coworkers[13] for calculating the partition function. The electronic information (energetic, structural, and vibrational) from the low

level PES was obtained with the MORATE 8.5.1 code,[14] which serves as an interface between MOPAC 5.09mn and POLYRATE 8.5.1.[15]

Several ab initio high level electronic structure calculations were carried out at the stationary points on the PES in order to correct the semiempirical low level electronic information. First, the low level moment-of-inertia determinants and frequencies at the stationary points were corrected by optimizing the geometries of the stationary points at two different levels of correlation. So, second-order Møller−Plesset perturbation theory (MP2)[16] was used with the 6-311G(2d,2p) basis set and the correlation-consistent polarized-valence triple-ζ (cc-pVTZ) basis set[17] of Dunning. MP2/6-311++G(2d,2p) optimizations were also performed for comparison purposes. In addition, geometry optimization of the stationary points was also carried out using quadratic configuration interaction including single and double excitations (QCISD)[18] with the 6-31G(d) and 6-311G(d,p) basis sets. Harmonic frequencies were computed at the ab initio optimized structures for the stationary points at the following levels: MP2/6-311G(2d,2p), MP2/6-311++G(2d,2p), MP2/cc-pVTZ, and QCISD/6-31G(d).

Second, higher level single-point energy calculations were carried out to correct the low level classical potential energy. On one hand, we employed the coupled cluster method, including single and double excitations and a perturbative estimate of the effect of triple excitations[19] with the 6-311++G-(2d,2p) basis set and the cc-pVTZ basis set at the MP2/6-311G-(2d,2p) and the MP2/cc-pVTZ geometries, respectively (namely, CCSD(T)/6-311++G(2d,2p)//MP2/6-311G(2d,2p) and CCSD-(T)//MP2/cc-pVTZ calculations). We also performed single-point energy calculations at the MP2/cc-pVTZ geometries using one of the general parametrizations of the SAC (scaling-all-correlation) method for semiempirical extrapolation of electronic structure calculations recently published by Truhlar et al.[20] In particular, we used the CCSD(T)-SAC/cc-pVTZ scheme with a scaling factor equal to 0.8928. Single-point energy calculations were also carried out at the QCISD(T)/6-311++G(2df,p)// QCISD/6-311G(d,p) level. A full electron correlation treatment was employed at the MP2, CCSD(T), QCISD, and QCISD(T) levels of correlation. Finally, the CBS-APNO[21a] and CBS−RAD[21b,21c] multilevel schemes were also used to correct the semiempirical low level PES. These multilevel techniques are practical methods for extrapolating finite basis set calculations to obtain estimates of the complete basis set (CBS) limit.

All these ab initio calculations were done using GAUSSIAN 94 and GAUSSIAN 98 quantum mechanical suite of programs.[22]

Dynamics Calculations. Reaction rate constants were calculated by variational transition state theory with interpolated optimized corrections (VTST-IOC).[23] Following this methodology, the correction procedures were applied to the classical energies, moment-of-inertia determinants and frequencies along the low level MEP calculated by using straight direct dynamics. The corrections are calibrated such that the corrected results match the high level values at the stationary points, and they correspond to interpolating these corrections at other points.

The high level classical potential energy along the MEP was interpolated with a single Eckart function. The generalized harmonic vibrational frequencies along the MEP were corrected with the "interpolated corrections-additive" (ICA) scheme. An adiabatic type of correlation along the MEP was employed for interpolating the frequencies of the saddle point, reactants, and products. In the hindered rotor approximation used in this paper for describing the lowest mode of vibration at the stationary points and along the MEP, we need the reduced moments of inertia to calculate the partition functions. Since the reduced moment of inertia should not change very much in the region close to the saddle point (which is the only region where the reduced moment of inertia is typically needed), we have approximated the high level reduced moment of inertia of the hindered rotor by its value at the saddle point. Rotations are treated by the classical rigid rotor approximation. The high level determinant of moment of inertia tensor, which is the product of the principal moments of inertia, is obtained from the low level values along the MEP with the correction eqs 15 and 16 of ref 23a. For the electronic partition function we have assumed no low-lying excited state of the $^2A_1$ saddle point, but we have included the $^2\Pi_{1/2}$ excited state (140 cm^{-1}) of OH in the reactant partition function. The reaction path symmetry factor for this reaction, which accounts for the number of equivalent reaction paths, was calculated according to the general expression:[24]

$$\sigma(s) = \frac{n\sigma^R}{\sigma^{GT}(s)}$$

where n is the number of identical transition states, σ^R is the usual rotational symmetry number for the reactants (it is the product of these symmetry numbers if there are two molecular reactants), and $\sigma^{GT}(s)$ is the usual rotational symmetry number for the generalized transition state at s. In our application, as usual, σ^{GT} is independent of s. In the perprotio reaction, the symmetry point groups for reactants are C_{2v} for CH_2F_2 and $C_{\infty v}$ for OH, yielding $\sigma^R = 2$. The symmetry point group for the transition state is C_1, leading to $\sigma^{GT} = 1$. In this case, though, $n = 2$ because at the transition state the hydroxyl radical has two indistinguishable reaction paths of approach depending on which of the two fluorine atoms forms a hydrogen bond with the hydrogen atom of the incoming radical.

We have employed canonical unified statistical transition state theory (CUS)[25] plus multidimensional tunneling (MT) contributions for calculating the rate constants over a wide range of temperatures for the OH + CH_2F_2 reaction. The CUS calculations have been necessary because the free energy profiles of the perprotio reaction present two maxima around the saddle point location. The small-curvature tunneling (SCT)[26] semiclassical adiabatic ground-state approximation, the large-curvature tunneling (LCT)[25a,27] correction and the microcanonical optimized multidimensional (μOMT)[28] method have been used to correct for tunneling. For the LCT calculations, we have compared the large-curvature ground-state approximation, version 3 (LCG3),[27,29] with the recently developed large-curvature ground-state approximation, version 4 (LCG4)[30] that was developed to improve the treatment of the anharmonic potentials encountered along the low-energy corner-cutting tunneling paths. The final μOMT tunneling transmission coefficients (using the LCG4 algorithm for large-curvature tunneling corrections) have been calculated allowing the system to reach all the accessible vibrational excited states into which tunneling proceeds. The effective potential in the nonadiabatic region has been corrected using a linear or a quadratic type of expression depending on the magnitude of the corrections in different regions.

All the dynamics calculations have been carried out with the MORATE 8.5.1 code.[14]

Results and Discussion

In this section, the results corresponding to the electronic calculations on the CH_2F_2 + OH reaction are first presented. In a second subsection the dynamical results will be described.

TABLE 1: Classical Potential Energy Barrier Height, Adiabatic Barrier at the Saddle Point Structure, and Classical Reaction Energy at Different Levels of Electronic Structure Calculations

energies[a]	$V^{\neq}$	$\Delta V_a^{G\neq}$	ΔV
AM1	8.4	7.0	−34.5
PM3	7.3	4.8	−29.2
MP2/6-311G(2d,2p)	8.6	6.7	−17.8
MP2/6-311++G(2d,2p)	9.5	7.5	−19.4
MP2/cc-pVTZ	7.8	5.9	−18.7
CCSD(T)/6-311++G(2d,2p)//MP2/6-311G(2d,2p)	6.8	4.9	−14.8
QCISD(T)/6-311++G(2df,p)//QCISD/6-311G(d,p)	5.8	3.7	−14.5
CCSD(T)//MP2/cc-pVTZ	5.1	3.3	−14.5
CCSD(T)-SAC//MP2-cc-pVTZ	2.9	1.1	−15.9
CBS-APNO	3.7	1.5	−16.9
CBS−RAD	3.4	1.3	−16.5

[a] In kcal/mol.

Electronic Structure Calculations. In Table 1 the classical potential energy barrier height, the adiabatic barrier at the saddle point structure, and the classical reaction energy are presented at different levels of electronic structure calculations. The experimental classical reaction energy, calculated using the experimental heats of formation[31a] for reactants and products, at 0 K, and the experimental frequencies[31b] for CH_2F_2, OH, and H_2O along with the QCISD/6-311G(d,p)[QCISD/6-31G(d)] zero point energy for CHF_2, is -16.3 ± 2.0 kcal/mol. The large error bar in the experimental exoergicity comes mainly from the experimental uncertainty in the enthalpy of formation for CHF_2. It can be seen in Table 1 (third column) that the AM1 and PM3 semiempirical methods predict reaction energies that are 18.2 and 12.9 kcal/mol too exoergic, respectively. The MP2/6-311G-(2d,2p) exoergicity is within the experimental range although in the lower limit. When diffuse functions are added to the basis set at the MP2/6-311++G(2d,2p) level, the reaction energy turns out to be larger than the experimental value by 3.1 kcal/mol, whereas the MP2/cc-pVTZ value is only 2.4 kcal/mol too exoergic. The X//Y dual-level classical reaction energies, where X stands for CCSD(T) or QCISD(T) single-point energy calculations, are within the experimental range but at the upper limit. The three multilevel single-point energy calculations, namely, the SAC procedure and the two extrapolating CBS techniques predict classical reaction energies within the experimental range giving better exoergicities than any of the single-level calculations. The most accurate value of −16.5 kcal/mol is obtained with the CBS−RAD method. Several results in the literature have already proved that these multilevel techniques (along with G2, G3, and their many variants[32]) and also multicoefficient correlation methods such as multicoefficient scaling all correlation (MCSAC)[33] and multicoefficient correlation methods (i.e., MCCM,[33] MC-QCISD,[34] MCG2,[35] MCG3[36]) are powerful electronic structure techniques for calculating high-accuracy thermochemistry for small to medium-sized systems. However, the doubt still remains when one has to decide which electronic structure methodology is the most adequate to calculate saddle point energies, especially in open-shell radical reactions. In Table 1, the classical and adiabatic barrier height values (columns 2 and 3, respectively) at the saddle point structure show an important dispersion among the different levels of calculation employed in the present work. The ab initio lowest level calculations (that is, the MP2 values) and the semiempirical methods give the highest barriers (from 7.3 to 9.5 kcal/mol). When higher level single-point energy corrections are included by means of dual-level X//Y computations, the classical barrier heights decrease by 1.8 kcal/mol at the CCSD-(T)/6-311++G(2d,2p)//MP2/6-311G(2d,2p) level and by 2.7 kcal/mol at the CCSD(T)//MP2/cc-pVTZ level. The lowest classical barriers, though, are given by the three multilevel techniques. The adiabatic barriers are around 2 kcal/mol lower at each level of calculation than the corresponding classical barrier heights.

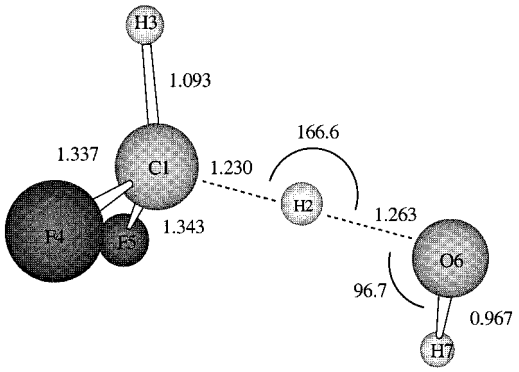

Figure 1. Saddle point structure located at the QCISD(T)/6-311++G-(2df,p)//QCISD/6-311G(d,p) level. Bond lengths are in angstroms and bond angles in degrees.

TABLE 2: Main Geometrical Parameters of the Saddle Point Structure at Different Levels of Electronic Structure Calculations[a]

	$d(C_1-H_2)$	$d(H_2-O_6)$	$\alpha(C_1-H_2-O_6)$	$\Phi(H_7-O_6-C_1-F_4)$
PM3	1.236	1.352	168.8	53.4
MP2/6-311G(2d,2p)	1.193	1.294	164.2	13.4
MP2/6-311G++(2d,2p)	1.191	1.302	169.2	21.1
MP2/cc-pVTZ	1.183	1.305	167.7	15.6
QCISD/6-31G(d)	1.261	1.246	164.5	21.1
QCISD/6-311G(d,p)	1.230	1.263	166.6	18.5

[a] Distances are given in Å and angles in degrees.

From the comparison between the semiempirical results with the experimental data and the ab initio values, the AM1 method was discarded as the low level PES for carrying out the dual-level direct dynamics study of the OH + CH_2F_2 reaction. For this reason, we will refer from now on to the PM3 semiempirical results only.

The optimized structures for the reactants (CH_2F_2 + OH) and products (CHF_2 + H_2O) at the ab initio levels (namely, MP2/6-311G(2d,2p), MP2/6-311++G(2d,2p), MP2/cc-pVTZ, QCISD/6-31G(d), and QCISD/6-311G(d,p)) do not significantly differ. The main discrepancies in bond lengths are only of 0.01 Å and the discrepancy in bond angles attain a maximum value of 1.6° degrees (observed only in the water molecule angle). These ab initio results agree well with experiment, with the main differences observed for the water molecule. The semiempirical PM3 method tends to give shorter C−F and O−H distances (especially in the OH molecule) and somewhat longer C−H bonds. In particular, the main difference between semiempirical and ab initio geometries is found in the FCH angle of the CHF_2 radical which has a value of 121.3° at the PM3 level and of around 113.8 ° at the ab initio level.

The saddle point structure at the QCISD/6-311G(d,p) level is depicted in Figure 1. Table 2 presents a comparison of the main geometrical parameters of the saddle point structure at the different levels of electronic structure calculation used in this work for optimization. All these saddle point geometries have an $\Phi(H_7-O_6\cdots C_1-F_4)$ dihedral angle somewhat different from zero, meaning than none of them is exactly eclipsed. The main discrepancy in the saddle point structures of Table 2 comes from the C_1-H_2 and H_2-O_6 bond distance values. At the PM3 and the MP2 optimized saddle point structures, the C_1-H_2 distance is shorter than the H_2-O_6 distance. However, at the

TABLE 3: Harmonic Frequencies for the Saddle Point Structure at Different Levels of Electronic Structure Calculations

level	saddle point harmonic frequencies[a]	zero point energy[b]
PM3	3993, 2921,1568,1428,1231,1018,981, 789, 691, 565, 488, 109, 81, 26, 2638i	22.7
MP2/6-311G-(2d,p)	3821, 3175, 1578, 1417, 1325, 1180, 1157, 1151, 878, 661, 529, 158, 146, 98, 2213i	24.7
MP2/6-311-++G(2d,2p)	3811, 3180, 1532, 1407, 1288, 1161, 1150, 1140, 855, 690, 529, 156, 132, 71, 2238i	24.5
MP2/cc-pVTZ	3806, 3161, 1565, 1430, 1321, 1191, 1175, 1167, 868, 721, 541, 163, 143, 91, 2025i	24.8
QCISD/6-31G(d)	3684, 3151, 1607, 1410, 1284, 1210, 1175, 1115, 847, 571, 494, 154, 132, 92, 2161i	24.2

[a] In cm^{-1}. [b] In kcal/mol.

MP2 optimized geometries the two bond distances, C_1-H_2 and H_2-O_6, are shorter than the corresponding bond distances at the PM3 saddle point. The QCISD saddle point structures present larger or approximately equal C_1-H_2 bond distances and smaller H_2-O_6 bond distances than the semiempirical and MP2 geometries. However, while the C_1-H_2 bond distance is 0.015 Å longer than the H_2-O_6 distance using the 6-31G(d) basis set, the QCISD/6-311G(d,p) level of optimization (like at the semiempirical and at the MP2 levels) gives a C_1-H_2 bond distance 0.033 Å shorter than the H_2-O_6 bond distance. These trends of the C_1-H_2 and H_2-O_6 bond lengths were already reported by Truhlar and co-workers[37] for the hydrogen abstraction reaction CH_4 + OH. In that paper, the authors pointed out that, interestingly, the RUCCSD(T), UCCSD(T), UQCISD(T), UCCSD, and UQCISD geometries for the CH_4 + OH saddle point are in good agreement. The authors conclude that these methods should be preferred to UMP2 and ROMP2 for open-shell transition state geometry optimizations.

The harmonic frequencies for the saddle point structure at the different optimization levels are presented in Table 3 along with the corresponding zero point energies (ZPEs). PM3 and QCISD/6-31G(d) ZPEs differ by 1.5 kcal/mol, and the imaginary frequency is smaller by 477 cm^{-1} at the QCISD level. The MP2 ZPEs are all larger than the QCISD ZPEs (from 0.6 kcal/mol of energy difference, compared to the MP2/cc-pVTZ ZPE, to 0.3 kcal/mol of energy difference, compared to the MP2/6-311++G(2d,2p) result). In contrast, while MP2/6-311G(2d,-2p) and MP2/6-31++G(2d,2p) imaginary frequencies are greater than the corresponding QCISD/6-31G(d) imaginary frequency, the MP2/cc-pVTZ imaginary frequency is 136 cm^{-1} lower. For the dynamics calculations within the harmonic approximation, the frequencies were scaled to include anharmonicity effects in a parametrized way. The following scale factors were adopted: 0.9748[38] at the MP2/6-311G(2d,2p) level; 0.9790[20] at the MP2/cc-pVTZ level, and 0.9776[38] at the QCISD/6-31G(d) level.

As it was explained in the Method of Calculation section, all vibrations were treated in the harmonic approximation except for the lowest vibrational mode. The partition function for the internal rotation corresponding to this lowest vibrational mode was evaluated at the saddle point structure using the general hindered partition function expressions of Truhlar and co-workers.[13] The scheme adopted in this work is named full CW. Following this scheme, the moment of inertia for the internal rotation was calculated using Pitzer's curvilinear algorithm.[39] The barrier to internal rotation was calculated on the MP2/6-311G(2d,2p) PES taking the $\Phi(H_7-O_6\cdots C_1-F_4)$ dihedral angle as the reaction coordinate. The computed energetic profile is depicted in Figure 2. Two nonsymmetrically equivalent minima appear along the rotational profile, each with symmetry number

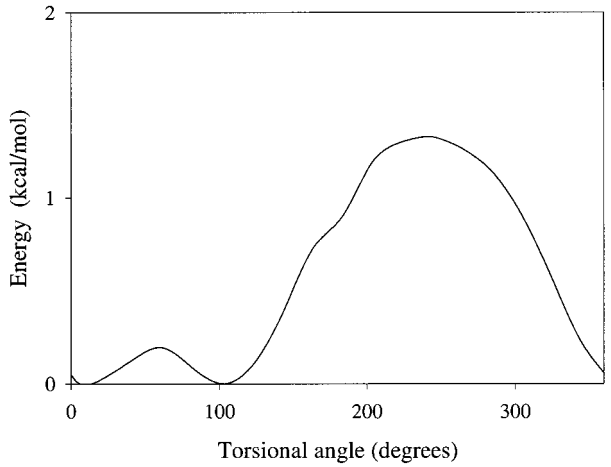

Figure 2. Calculated classical energy profile along the torsional angle $\Phi(H_7-O_6\cdots C_1-F_4)$ for the hindered rotor mode at the MP2/6-311G-(2d,2p) level.

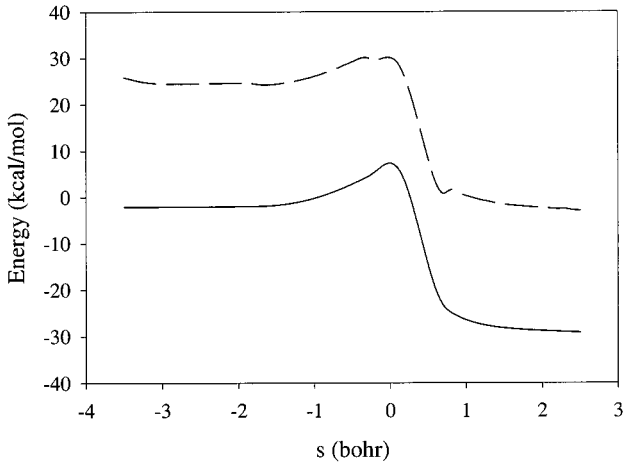

Figure 3. Classical potential energy (solid line) and vibrational adiabatic ground-state energy (dash-dash line) along the PM3 minimum energy path.

1. The two calculated internal barriers are 0.2 and 1.3 kcal/mol. The same moment of inertia for internal rotation has been adopted for both minima, and the values obtained at the different levels of optimization used in the direct dynamics calculations are 13870 au at the PM3 level, 8981.6 au at the MP2/6-311G-(2d,2p) level, 7680.8 au at the MP2/cc-pVTZ level, and 5756.3 au at the QCISD/6-311G(d,p) level. The two harmonic frequencies associated to the two rotational barriers are calculated from eq 5 of ref 13. In the dynamics calculations, this hindered rotor treatment will increase the rate constant values at all the studied temperatures as compared to the harmonic approach, being this effect more significant as temperature goes up.

The low-level PM3 MEP along with the corresponding adiabatic curve are shown in Figure 3. Two hydrogen-bonded intermediate complexes are present on the reactants and products sides of the MEP. The PM3 geometries for those two complexes are depicted in Figure 4. The reactant complex geometry is similar to the saddle point structure with the difference that the hydroxyl radical has moved away although a hydrogen bond (O···H distance of 1.779 Å) is maintained between the oxygen atom of OH and the hydrogen atom that is abstracted at the transition state. The hydrogen-bond interaction provides a stabilization energy to the complex of 2.1 kcal/mol. In the product complex the water molecule is already formed and has rotated in order to establish a hydrogen bond with one of the two fluorine atoms of the CHF_2 moiety, the F···H distance being

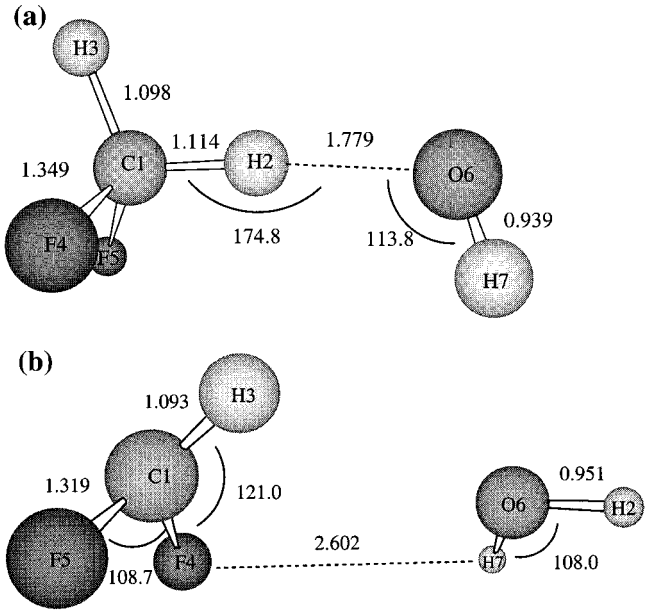

Figure 4. van der Waals complex structures corresponding to the reactants region (a) and to the products region (b) located on the PM3 potential energy surface. Bond distances are in angstroms and bond angles in degrees.

of 2.602 Å. The product complex stabilization is of −31.4 kcal/mol with respect to reactants. It has to be pointed out here that the reaction complexes were not used for correcting the low level MEP since the values of the reaction coordinate for the reactant and product side complexes were not determined due to convergence problems of the algorithm for following the MEP. However, it has already been described in the literature[40] the important dynamical role of prereaction complexes in hydrogen abstraction reactions. In particular, tunneling effects are very sensitive to the existence of reactant side complexes because they can significantly modify the shape of the adiabatic energy profile. For this reason, the effect of the reactant complex was partially taken into account by calculating the range parameter (L) for the Eckart function with respect to the energies of the prereaction complexes. That is, we approximated the range parameter L of the Eckart correction function for V_{MEP} as follows. First we fitted the low level V_{MEP} to an Eckart function at the three stationary points (reactants, saddle point, and products) and at one additional point at $s = -0.26$ bohr (in an exoergic reaction the fourth point needed for the fitting of the Eckart function is taken from the reactant region on the MEP) that satisfies the following relationship:

$$V_{LL}^{\neq} - V_{MEP,LL}\,(s = -0.26\ \text{bohr}) = 1/2\,(V_{LL}^{\neq} - V_{C,LL})$$

where $V_{LL}^{\neq}$ stands for the classical barrier height at the low level (PM3) saddle point, $V_{MEP,LL}(s)$ corresponds to the classical potential energy on the MEP at s, and $V_{C,LL}$ is the classical potential energy at the reactant complex. This fitting is then discarded and only the range parameter obtained, $L = 0.27$ bohr, is kept for the Eckart correction function (see eqs 5 of ref 23). The low level adiabatic profile (see Figure 3) presents two maxima in the region close to the saddle point. These maxima also appear on the low level free energy profiles at higher temperatures, which justifies the use of CUS theory for the dynamics calculations, as we have already stated in the Method of Calculation section.

Dynamics Calculations. We have carried out several dual-level dynamics calculations using the VTST-IOC approach. These calculations will be denoted as

I. CCSD(T)/6-311++G(2d,2p)//MP2/6-311G(2d,2p)///PM3

II. CCSD(T)//MP2/cc-pVTZ///PM3

III. CCSD(T)-SAC//MP2/cc-pVTZ///PM3

IV. QCISD(T)/6-311++G(2df,p)//QCISD/6-311G(d,p)[QCISD/6-31G(d)]///PM3

V. CBS-APNO///PM3

VI. CBS−RAD///PM3

Truhlar and co-workers[41] called these kind of calculations triple-slash dynamics because of their nomenclature. In particular, W//X///Z means that the reaction path data (and the reaction-swath data if large-curvature or optimized multidimensional tunneling calculations are carried out) is calculated at a lower-level Z (PM3 in our case) and stationary points are calculated at a higher level W//X. As usual, W//X refers to optimization (and frequencies if applicable) at level X with single-point energies calculated at higher level W. They also introduced the convenient notation X[Y], which denotes geometry optimization and energy calculated at level X with frequencies at level Y. This, of course, involves a geometry optimization at level Y as an intermediate step in calculating frequencies, but this geometry is replaced by the level-X geometry for further stages.

The rate constants calculated by the six dual-level approaches (I−VI) using CUS theory and including tunneling corrections with the μOMT method (calculated using LCG4 algorithm for large-curvature corrections) have been calculated and compared to experimental results. The numerical values for all these rate constants are given in Table 4. From this table it can be observed that method I underestimates the rate constants at all the temperatures, especially in the temperature range 325−425 K. On the other hand, methods III, V, and VI overestimate the rate constants at all temperatures but most significantly below 300 K (with deviation factors greater than 9.0). The two methods in Table 4 that give the best agreement with experimental results are methods II and IV. The rate constants calculated with these two dual-level methodologies are shown in Figure 5 along with the experimental results. The dual-level dynamics calculations using method II (CCSD(T)//MP2/cc-pVTZ///PM3) slightly overestimate the experimental rate constants in the whole range of temperatures (except at 425 K), although the deviation increases as temperature goes down. This deviation remains within a factor of approximately 1.0 to 1.4 (also depending which experimental results we take as reference) down to 300 K and becomes more important at lower temperatures. On the other hand, method IV (QCISD(T)/6-311++G(2df,p)//QCISD/6-311G(d,p)[QCISD/6-31G(d)]///PM3) slightly underestimates (within a factor of 1.0 to 1.1) the experimental rate constants from 500 or 475 K to 350 K and progressively overestimates the experimental results from 300 K (where the factor of deviation is only of 1.1−1.2) to 210 K (where the factor of deviation increases up to 3.1−3.7).

In Table 5 the rate constants as a function of temperature obtained using the dual-level dynamics method IV are factorized in their different contributions. As a first point, it is worth mentioning the important variational effects that are present in the hydrogen abstraction reaction under study. The differences between the conventional transition-state rate constants (k^{TST}), given in column 2 of Table 5, and the variational transition-

TABLE 4: Rate Constants (cm^3 $molec^{-1}$ s^{-1})calculated for Six Dual-Level Approaches Using CUS Theory and Including μOMT Tunneling Corrections (power of 10 in parentheses)

T (K)	I[a]	II[b]	III[c]	IV[d]	V[e]	VI[f]	expt.[g]	expt.[h]
210	1.14(−15)	5.58(−15)	4.51(−14)	4.42(−15)	3.48(−14)	5.04(−14)	1.43(−15)	1.18(−15)
225	1.35(−15)	6.49(−15)	5.22(−14)	5.19(−15)	4.10(−14)	5.91(−14)	2.28(−15)	1.94(−15)
250	1.82(−15)	8.59(−15)	6.64(−14)	6.99(−15)	5.32(−14)	7.59(−14)	4.38(−15)	3.86(−15)
275	2.45(−15)	1.14(−14)	8.29(−14)	9.41(−15)	6.71(−14)	9.55(−14)	7.49(−15)	6.77(−15)
300	3.57(−15)	1.49(−14)	1.02(−13)	1.26(−14)	8.50(−14)	1.18(−13)	1.17(−14)	1.08(−14)
325	3.88(−15)	1.95(−14)	1.24(−13)	1.67(−14)	1.05(−13)	1.43(−13)	1.70(−14)	1.61(−14)
350	5.25(−15)	2.51(−14)	1.49(−13)	2.19(−14)	1.28(−13)	1.73(−13)	2.35(−14)	2.27(−14)
375	7.03(−15)	3.19(−14)	1.77(−13)	2.83(−14)	1.55(−13)	2.04(−13)	3.11(−14)	3.04(−14)
400	9.33(−15)	4.08(−14)	2.04(−13)	3.50(−14)	1.81(−13)	2.41(−13)	3.98(−14)	3.94(−14)
425	1.22(−14)	4.83(−14)	2.37(−13)	4.59(−14)	2.14(−13)	2.83(−13)	4.94(−14)	4.95(−14)
450	1.59(−14)	6.16(−14)	2.80(−13)	5.70(−14)	2.56(−13)	3.37(−13)	5.99(−14)	6.06(−14)
475	2.03(−14)	7.46(−14)	3.21(−13)	6.99(−14)	2.98(−13)	3.89(−13)	7.11(−14)	7.27(−14)
500	2.57(−14)	8.95(−14)	3.66(−13)	8.49(−14)	3.44(−13)	4.47(−13)	8.30(−14)	8.56(−14)

[a] CCSD(T)/6-311++G(2d,2p)//MP2/6-311G(2d,2p)///PM3. [b] CCSD(T)//MP2/cc-pVTZ///PM3. [c] CCSD(T)-SAC//MP2/cc-pVTZ///PM3. [d] QCISD(T)/6-311++G(2df,p)//QCISD/6-311G(d,p)[QCISD/6-31G(d)]///PM3. [e] CBS-APNO///PM3. [f] CBS−RAD///PM3. [g] $k(T) = (1.57 \pm 0.21) \times 10^{-12} \exp(-1470 \pm 100)$. The error bars are 2σ and include systematic errors (ref 42). [h] $k(T) = 1.9 \times 10^{-12} \exp(-1550 \pm 200)$; $f(298\ \mathrm{K}) = 1.2$ (ref 31a).

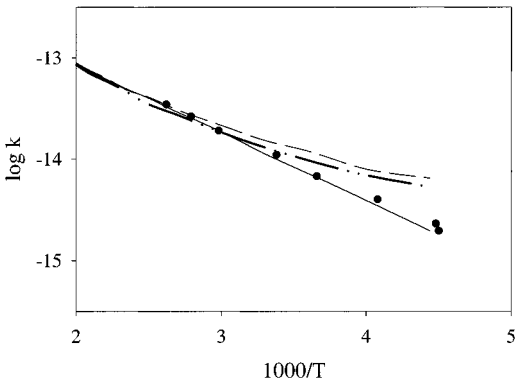

Figure 5. Arrhenius plots for the calculated rate constants at the QCISD(T)/6-311++G(2df,p)//QCISD/6-311G(d,p)[QCISD/6-31G(d)]/// PM3 level (dash-dot-dot line) and at the CCSD(T)//MP2/cc-pVTZ/// PM3 level (dash-dash line). Experimental data: rate constants from ref 42 (black circles) and recommended equation from ref 31a (solid line). Rate constants are in cm^3 $molec^{-1}$ s^{-1}.

TABLE 5: Factorization of the Rate Constants Obtained Using the Dual-Level Dynamics Method IV[a]

T (K)	k^{TST}	k^{CVT}	k^{CUS}	$k^{CUS/SCT}$	$k^{CUS/LCG3}$	$k^{CUS/LCG4}$
210	4.36(−16)	8.70(−17)	7.23(−17)	3.65(−15)	4.35(−15)	3.35(−15)
225	7.70(−16)	1.72(−16)	1.41(−16)	4.34(−15)	5.52(−15)	4.06(−15)
250	1.73(−15)	4.48(−16)	3.65(−16)	5.99(−15)	8.24(−15)	5.69(−15)
275	3.39(−15)	9.95(−16)	8.07(−16)	8.25(−15)	1.19(−14)	7.86(−15)
300	6.04(−15)	1.94(−15)	1.58(−15)	1.13(−14)	1.68(−14)	1.07(−14)
325	9.98(−15)	3.47(−15)	2.83(−15)	1.53(−14)	2.30(−14)	1.44(−14)
350	1.55(−14)	5.75(−15)	4.72(−14)	2.02(−14)	3.06(−14)	1.91(−14)
375	2.30(−14)	8.99(−15)	7.42(−14)	2.65(−14)	3.99(−14)	2.49(−14)
400	3.27(−14)	1.34(−14)	1.08(−14)	3.30(−14)	4.94(−14)	3.11(−14)
425	4.50(−14)	1.91(−14)	1.62(−14)	4.37(−14)	6.46(−14)	4.12(−14)
450	6.03(−14)	2.63(−14)	2.25(−14)	5.46(−14)	7.96(−14)	5.14(−14)
475	7.90(−14)	3.53(−14)	3.03(−14)	6.73(−14)	9.67(−14)	6.35(−14)
500	1.01(−13)	4.62(−14)	3.99(−14)	8.21(−14)	1.16(−13)	7.76(−14)

[a] All the results are given in cm^3 $molec^{-1}s^{-}1$ (power of 10 in parentheses).

state rate constants (k^{CVT}), given in column 3 of Table 5, are caused by these marked variational effects. At all temperatures the variational transition state location, specified by the value of $s^{*CVT}(T)$, moves toward the reactant side of the PES. The values of $s^{*CVT}(T)$ range from −0.342 bohr at 210 K to −0.322 bohr at 500 K. The variational effect goes from a value of 0.199 at 210 K to a value of 0.456 at 500 K. Note that the variational effect is defined as the ratio between variational CVT and conventional TST rate constants. Significant variational effects have also been detected in all the other hydrogen abstraction reactions from methane or fluoromethanes studied in the past

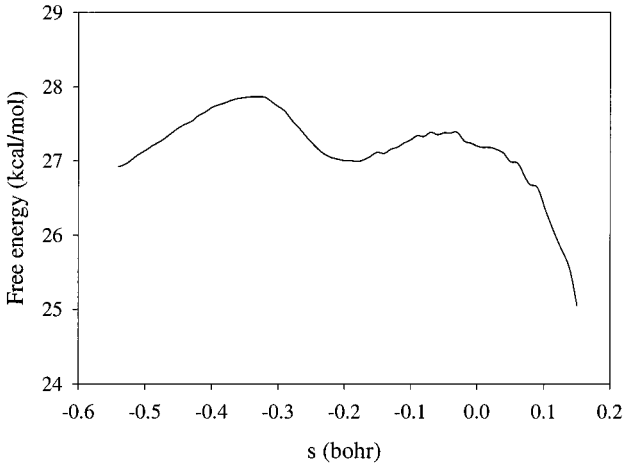

Figure 6. Free energy profile at 210 K calculated at the QCISD(T)/6-311++G(2df,p)//QCISD/6-311G(d,p)[QCISD/6-31G(d)]///PM3 level.

with VTST, although the magnitude of those variational effects is sensitive to the quality of the low level PES used for the dynamics calculations.[4,23a,24c,43−46] Moreover, in TST studies of these reactions, some of the deviations obtained between theoretical and experimental rate constants were said to reflect the importance of variational effects that were not considered in those studies.[5]

In Figure 6 the free energy profile obtained with method IV at 210 K is depicted as an example. It can be observed (as it was already detected on the low level free energy profiles) the existence of two maxima of similar height separated by a minimum of free energy. Therefore, the rate constants were finally calculated using the canonical unified statistical model (CUS). The comparison of columns 3 and 4 of Table 5 shows that the two free energy maxima in the variational calculation provoke a decrease of the rate constants at all temperatures.

The last three columns of Table 5 detail the numerical values of the rate constants when tunneling is included by means of three different transmission coefficient expressions: SCT in column 5, LCG3 in column 6, and LCG4 in column 7. Several important issues concerning tunneling effects can be deduced from the comparison of these transmission coefficient values. First, the comparison of the LCG3 and LCG4 transmission coefficients shows, as it is expected by the mathematical definition of LCG4 algorithm, that LCG4 method predicts less tunneling than do LCG3 calculations, although the difference represents only a factor of 1.30 at the lowest temperature. Second, tunneling effects predicted by the SCT algorithm are

more important at all temperatures than those given by the LCG4 method, thus reflecting that the dominant tunneling mechanism in the dual level calculations is the small-curvature tunneling. Note that in the μOMT approach, used for calculating the final rate constants given in Table 4, at each total energy, the larger of the SCT or LCG4 tunneling probabilities is taken as the best estimate. Third, it is worth pointing out the rapid increase of tunneling transmission coefficients below 300 K.

Summary and Final Remarks

In this paper we have calculated theoretically the reaction rate constants of the hydrogen abstraction of CH_2F_2 by OH from 210 to 500 K. Recently, Schwartz et al.[5] have achieved a quite good agreement with the experimental rate constants for that reaction in a wide range of temperatures using conventional transition state theory along with Eckart tunneling factors and a suitable fitting of the classical energy barrier (a final value of 6.3 kcal/mol was obtained) in order to match the experimental rate constant at 298 K. However, this reaction will be a challenge for the theoreticians until we are able to obtain accurate rate constants excluding any adjustment to the experimental rate constants.

To this aim we have used here the current state-of-the-art methods for both the electronic structure and the dynamics calculations, no fitting to the experimental rate constants having been performed. That includes variational transition state theory with interpolated optimized corrections at several ab initio high electronic levels along with multidimensional semiclassical tunneling calculations. More concretely, we have used the canonical unified statistical model, the recently developed full CW general hindered partition function expressions, to calculate the partition function for the internal rotation corresponding to the lowest vibrational mode, and the even more recently developed LCG4 method to calculate the large-curvature tunneling corrections and the microcanonical optimized multidimensional tunneling corrections.

Our calculations at the QCISD(T)/6-311++G(2df,p)//QCISD/6-311G(d,p)[QCISD/6-31G(d)]///PM3 and the CCSD(T)//MP2/cc-pVTZ///PM3 levels reproduce quite well the experimental rate constants from 500 to 250 K, and slightly overestimate them from 250 to 210 K. The classical energy barriers turn out to be, respectively, 5.8 or 5.1 kcal/mol. We have to underline that we have found quite significant variational effects at all the temperatures. Then conventional transition state theory does not seem to be adequate for this reaction.

The behavior of the rate constants at low temperatures still defies the theory. The overestimation of our theoretical rate constants with respect to the experimental ones below 250 K indicates that tunneling is somewhat overvalued, although the new LCG4 method has been used to account for the large-curvature tunneling corrections. The exaggeration of the tunneling could be due to the fact that the semiempirical PM3 as a low electronic level provides a too narrow minimum energy path. This deficiency poses serious arguments to the validity of the fourth conclusion stated in our previous work on the CH_3F + OH reaction, where dual-level dynamics based on semiempirical molecular orbital calculations were qualified as a very promising tool for computing dynamical properties in reactions with halocarbons. As a matter of fact, we have confirmed that the MP2/6-311G(2d,2p) level leads to a somewhat wider reaction path. At this MP2 level, the two hydrogen-bonded intermediate complexes are also present in the reactant and product sides of the MEP. The MP2 product complex is very similar to the PM3 one, whereas the MP2 reactant complex involves a double hydrogen bond including now an F···H interaction. In a recent paper, Hu and co-workers[46] have also found for the hydrogen abstraction reaction of CH_3F by OH that the MP2/6-31+G(d,p) MEP is much wider than the PM3 one. In effect, Hu and co-workers have achieved an important improvement in order to get a more reliable barrier width. However, those authors, even using MP2/6-31+G(d, p) as a low electronic level, have needed to take the classical energy barrier height as an adjustable parameter to fit the experimental data (their best estimate of the classical energy barrier height is between 2.80 and 3.06 kcal/mol, which is significantly lower than those by all previous theoretical studies). Then it seems that the calculation without any fitting of accurate rate constants for the hydrogen abstraction reaction of CH_2F_2 by OH at low temperatures is still an open point. Additional theoretical work in this direction is now in progress in our laboratory.

Acknowledgment. We thank DGESIC for financial support through project No. PB98-0915. The use of the computational facilities of the CESCA and CEPBA coordinated by the C[4] is gratefully acknowledged.

References and Notes

(1) Montreal Protocol on Substances that Deplete the Ozone Layer, United Nations Environmental Programme, 1987.

(2) (a) WMO, Atmospheric Ozone, 1989, Scientific Assesment of Stratospheric Ozone, World Meteorological Organization, Global Ozone Research and Monitoring Project Report No. 20, Volume II, Appendix; AFEAS Report, Geneva, Switzerland. (b) Wayne, R. P. In *Chemistry of Atmospheres*, 3rd ed.; Oxford Science Publications: Oxford, NY, 2000; pp 230, 437.

(3) Wallington, T. J.; Schneider, W. F.; Nielsen, O. J.; Sehested, J.; Worsnop, D. R.; De Bruyn, W. J.; Shorter, J. A. In *Halon Replacements Technology and Science*; Miziolek, A. W., Tsang, W., Eds.; ACS Symposium Series 611; American Chemical Society: Washington, DC, 1995; pp 16−30.

(4) Espinosa-García, J.; Coitiño, E. L.; González-Lafont, A.; Lluch, J. M. *J. Phys. Chem. A* **1998**, *102*, 10715.

(5) Schwartz, M.; Marshall, P.; Berry, R. J.; Ehlers, C. J.; Petersson, G. A. *J. Phys. Chem. A* **1998**, *102*, 10074.

(6) Korchowiec, J.; Kawahara, Sh-i.; Matsumura, K.; Uchimaru, T.; Sugie, M. *J. Phys. Chem. A* **1999**, *103*, 3548.

(7) Louis, F.; González, C. A.; Huie, R. E.; Kurylo, M. J. *J. Phys. Chem. A* **2000**, *104*, 8773.

(8) (a) Stewart, J. J. P. *J. Comput. Chem.* **1989**, *10*, 209. (b) Dewar, M. J.; Thiel, W. *J. Am. Chem. Soc.* **1977**, *99*, 4899, 4907.

(9) Dewar, M. J. S.; Zoebisch, E. G.; Healy, E. F.; Stewart, J. J. P. *J. Am. Chem. Soc.* **1985**, *107*, 3902.

(10) Page, M.; McIver, J. W., Jr. *J. Chem. Phys.* **1988**, *88*, 922.

(11) Stewart, J. J. P.; Rossi, I.; Hu, W.-P.; Lynch, G. C.; Liu, Y.-P.; Chuang, Y.-Y.; Li, J.; Cramer, C. J.; Fast, P. L.; Truhlar, D. G. MOPAC, version 5.0.9.mn; University of Minnesota, Minneapolis, 1999.

(12) Chuang Y.-Y.; Truhlar, D. G. *J. Phys. Chem. A* **1998**, *102*, 242.

(13) Chuang, Y.-Y.; Truhlar, D. G. *J. Chem. Phys.* **2000**, *112*, 1221.

(14) Chuang, Y.-Y.; Fast, P. L.; Hu, W.-P.; Lynch, G. C.; Liu, Y.-P.; Truhlar, D. G. MORATE 8.5.1; University of Minnesota, Minneapolis, 2001.

(15) Corchado, J. C.; Chuang, Y.-Y.; Fast, P. L.; Villà, J.; Hu, W.-P.; Liu, Y.-P.; Lynch, G. C.; Nguyen, K. A.; Jackels, C. F.; Melissas, V.; Lynch, B. J.; Rossi, I.; Coitiño, E. L.; Fernández-Ramos, A.; Steckler, R.; Garrett, B. C.; Isaacson, A. D.; Truhlar, D. G. POLYRATE 8.5.1; University of Minnesota, Minneapolis, 2000 (http://comp.chem.umn.edu/polyrate).

(16) (a) Hehre, W. J.; Radom, L.; Schleyer, P. v. R.; Pople, J. A. In *Ab Initio Molecular Orbital Theory*; Wiley: NY, 1986. (b) Møller, C.; Plesset, M. S. *Phys. Rev.* **1934**, *46*, 618.

(17) Dunning, T. H., Jr. *J. Chem. Phys.* **1989**, *90*, 1007.

(18) Pople, J. A.; Head-Gordon, M.; Raghavachari, K. *J. Chem. Phys.* **1987**, *87*, 5968.

(19) Raghavachari, K.; Trucks, G. W.; Pople, J. A.; Head-Gordon, M. *Chem. Phys. Lett.* **1989**, *157*, 479.

(20) Fast, P. L.; Corchado, J.; Sánchez, M. L.; Truhlar, D. G. *J. Phys. Chem.* **1999**, *103*, 3139.

(21) (a) Montgomery, J. A., Jr.; Ochterski, J. W.; Petersson, G. A. *J. Chem. Phys.* **1994**, *101*, 5900. (b) Ochterski, J. W.; Petersson, G. A.; Montgomery, J. A., Jr. *J. Chem. Phys.* **1996**, *104*, 2598. (c) Mayer, P. M.; Parkinson, C. J.; Radom, L. *J. Chem. Phys.* **1998**, *108*, 604.

(22) (a) Frisch, M. J.; Trucks, G. W.; Schlegel, H. B.; Gill, P. M. W.; Johnson, B. G.; Robb, M. A.; Cheeseman, J. R.; Keith, T. A.; Petersson, G. A.; Montgomery, J. A.; Raghavachari, K.; Al-Laham, M. A.; Zakrzewski, V. G.; Ortiz, J. V.; Foresman, J. B.; Cioslowski, J.; Stefanov, B. B.; Nanayakkara, A.; Challacombe, M.; Peng, C. Y.; Ayala, P. Y.; Chen, W.; Wong, M. W.; Andres, J. L.; Replogle, E. S.; Gomperts, R.; Martin, R. L.; Fox, D. J.; Binkley, J. S.; Defrees, D. J.; Baker, J.; Stewart, J. P.; Head-Gordon, M.; Gonzalez, C.; Pople, J. A. *Gaussian 94*; Gaussian Inc.: Pittsburgh, PA, 1995. (b) Frisch, M. J.; Trucks, G. W.; Schlegel, H. B.; Scuseria, G. E.; Robb, M. A.; Cheeseman, J. R.; Zakrzewski, V. G.; Montgomery, J. A.; Stratmann, R. E.; Burant, J. C.; Dapprich, S.; Millam, J. M.; Daniels, A. D.; Kudin, K. N.; Strain, M. C.; Farkas, O.; Tomasi, J.; Barone, V.; Cossi, M.; Cammi, R.; Mennucci, B.; Pomelli, C.; Adamo, C.; Clifford, S.; Ochterski, J.; Petersson, G. A.; Ayala, P. Y.; Cui, Q.; Morokuma, K.; Malick, D. K.; Rabuck, A. D.; Raghavachari, K.; Foresman, J. B.; Cioslowski, J.; Ortiz, J. V.; Stefanov, B. B.; Liu, G.; Liashenko, A.; Piskorz, P.; Kamaromi, I.; Gomperts, R.; Martin, R. L.; Fox, D. J.; Keith, T.; Al-Laham, M. A.; Peng, C. Y.; Nanayakkara, A.; Gonzalez, C.; Challacombe, M.; Gill, P. M. W.; Johnson, B. G.; Chen, W.; Wong, M. W.; Andres, J. L.; Head-Gordon, M.; Replogle, E. S.; Pople, J. A. *Gaussian 98*; Gaussian Inc.: Pittsburgh, PA, 1998.

(23) (a) Hu, W.-P.; Liu, Y.-P.; Truhlar, D. G. *J. Chem. Faraday Trans.* **1994**, *90*, 1715. (b) Chuang Y.-Y.; Truhlar, D. G. *J. Phys. Chem. A* **1997**, *101*, 3808.

(24) (a) Pechukas, P. *J. Chem. Phys.* **1976**, *64*, 1516. (b) Villà, J.; Corchado, J. C.; González-Lafont, A.; Lluch, J. M.; Truhlar, D. G. *J. Phys. Chem. A* **1999**, *103*, 5061. (c) Masgrau, L.; González-Lafont, A.; Lluch, J. M. *J. Chem. Phys.* **2001**, *114*, 2154.

(25) (a) Truhlar, D. G.; Isaacson, A. D.; Garrett, B. C. In *Theory of Chemical Reaction Dynamics*; Baer, M., Ed.; CRC Press: Boca Raton, FL, 1985; Vol.4, p 65. (b) Hu, W.-P.; Truhlar, D. G. *J. Am. Chem. Soc.* **1995**, *117*, 10726. (c) Hu, W.-P.; Truhlar, D. G. *J. Am. Chem. Soc*. **1996**, *118*, 860.

(26) (a) Liu, Y.-P.; Lynch, G. C.; Truong, T. N.; Lu, D.-h.; Truhlar, D. G.; Garrett, B. C. *J. Am. Chem. Soc.* **1993**, *115*, 2408. (b) Lu, D.-h.; Truong, T. N.; Melissas, V. S.; Lynch, G. C.; Liu, Y.-P.; Garrett, B. C.; Steckler, R.; Isaacson, A. D.; Rai, S. N.; Hancock, G. C.; Lauderdale, J. G.; Joseph, T.; Truhlar, D. G. *Comput. Phys. Commun.* **1992**, *71*, 235.

(27) Garrett, B. C.; Joseph, T.; Truong, T. N.; Truhlar, D. G. *Chem. Phys.* **1989**, *136*, 271.

(28) Liu, Y.-P.; Lu, D.-h.; González-Lafont, A.; Truhlar, D. G.; Garrett, B. C. *J. Am. Chem. Soc*. **1993**, *115*, 7806.

(29) Truong, T. N.; Lu, D.-h.; Lynch, G. C.; Liu, Y.-P.; Melissas, V. S.; Stewart, J. J. P.; Steckler, R.; Garrett, B. C.; Isaacson, A. D.; González-Lafont, A.; Rai, S. N.; Hancock, G. C.; Joseph, T.; Truhlar, D. G. *Comput. Phys. Commun.* **1993**, *75*, 143.

(30) Fernández-Ramos, A.; Truhlar, D. G. *J. Chem. Phys.* **2001**, *114*, 1491.

(31) (a) De More, W. B.; Golden, D. M.; Hampson, R. F.; Howard, C. J.; Kolb, C. E.; Molina, M. J. *Chemical Kinetics and Photochemical Data for Use in Stratospheric Modeling*; Evaluation Number 13, JPL Publication 00-3; JPL: Pasadena, CA, 2000. (b) Chase, M. W., Jr.; Davies, C. A.; Downey, J. R., Jr.; Frurip, D. J.; McDonald, R. A.; Syverud, A. N. *J. Phys. Chem. Ref. Data* **1985**, *14*, Suppl. 1 (JANAF tables).

(32) (a) Curtiss, L. A.; Raghavachari, K.; Trucks, G. W.; Pople, J. A. *J. Chem. Phys.* **1991**, *94*, 7221. (b) Curtiss, L. A.; Raghavachari, K.; Redfern, P. C.; Rassolov, V.; Pople, J. A. *J. Chem. Phys.* **1998**, *109*, 7764. (c) Curtiss, L. A.; Raghavachari, K.; Redfern, P. C.; Rassolov, V.; Pople, J. A. *J. Chem. Phys.* **1999**, *110*, 4703.

(33) (a) Fast, P. L.; Corchado, J. C.; Sánchez, M. L.; Truhlar, D. G. *J. Phys. Chem. A* **1999**, *103*, 5129. (b) Tratz, C. M.; Fast, P. L.; Truhlar, D. G. *PhysChemComm*. **1999**, *2*, article 14.

(34) Fast, P. L.; Truhlar, D. G. *J. Phys. Chem. A* **2000**, *104*, 6111.

(35) Fast, P. L.; Sánchez, M. L.; Corchado, J. C.; Truhlar, D. G. *J. Chem. Phys.* **1999**, *110*, 11679.

(36) Fast, P. L.; Sánchez, M. L.; Truhlar, D. G. *Chem. Phys. Lett.* **1999**, *306*, 407.

(37) Chuang, Y.-Y.; Coitiño, E. L.; Truhlar, D. G. *J. Phys. Chem. A* **2000**, *104*, 446.

(38) Scott, A. P.; Radom, L. *J. Phys. Chem.* **1996**, *100*, 16502.

(39) Pitzer, K. S.; Gwinn, W. D. *J. Chem. Phys.* **1942**, *10*, 428.

(40) (a) Masgrau, L.; González-Lafont, A.; Lluch, J. M. *J. Phys. Chem. A* **1999**, *103*, 1044. (b) Masgrau, L.; González-Lafont, A.; Lluch, J. M. *J. Comput. Chem.* **1999**, *20*, 1685.

(41) Corchado, J. C.; Espinosa-García, J.; Hu, W.-P.; Rossi, I.; Truhlar, D. G. *J. Phys. Chem.* **1995**, *99*, 687.

(42) Talukar, R.; Mellouki, A.; Gierczak, T.; Burkholder, J. B.; McKeen, S. A.; Ravishankara, A. R. *J. Phys. Chem.* **1991**, *95*, 5815.

(43) Melissas, V. S.; Truhlar, D. G. *J. Chem. Phys.* **1993**, *99*, 1013.

(44) Espinosa-García, J.; Corchado, J. C. *J. Chem. Phys.* **2000**, *112*, 5731.

(45) Masgrau, L.; González-Lafont, A.; Lluch, J. M. *J. Chem. Phys.* **2001**, *115*, 4515.

(46) Lien, P.-Y.; You, R.-M.; Hu, W.-P. *J. Phys. Chem. A* **2001**, *105*, 2391.